Available online at www.sciencedirect.com
SCIENCE DIRECT®
Chemical Physics Letters 397 (2004) 21–25
CHEMICAL PHYSICS LETTERS
www.elsevier.com/locate/cplett

Photofragment translational spectroscopy of nitric acid at 248 nm with VUV photoionization detection of products

M.J. Krisch [a,*], M.C. Reid [a], L.R. McCunn [a], L.J. Butler [a], J. Shu [b]

[a] Department of Chemistry, James Franck Institute, The University of Chicago, 5640 S. Ellis Avenue, Chicago, IL 60637, USA
[b] Chemical Sciences Division, Lawrence Berkeley National Laboratory, Berkeley, CA 94720, USA

Received 19 June 2004; in final form 19 June 2004
Available online 12 September 2004

Abstract

This study examines the 248-nm photodissociation of nitric acid (HNO_3) and characterizes the translational energy distribution of the nascent photofragments. Photofragment translational spectroscopy with VUV photoionization detection evidenced one product channel, cleavage of HNO_3 to form OH + NO_2, and established an upper limit on the contribution from the O + HONO formation channel of 3%. These data contribute an independent measurement to a literature debate regarding the branching between these two channels.

1. Introduction

Nitrogen oxides, molecules with complex electronic structure, test our ability to predict product branching and energy partitioning in photodissociation. Nitric acid photodissociation is a useful model system for examining electronic nonadiabaticity in reactions where individual orbital symmetry is not conserved along the reaction coordinate [1,2]. Furthermore, several groups have used HNO_3 as an OH precursor, generating interest in the OH quantum yield [3]. This study addresses a discrepancy in the literature regarding the product branching upon HNO_3 photodissociation at 248 nm.

The UV absorption spectrum of HNO_3 exhibits two broad peaks arising from electronic excitations centered on the NO_2 moiety. A strong absorption ($\sigma = 1.63 \times 10^{-17}$ cm^2) [4] centered at 185 nm is due to excitation to the bright $2^1A'$ state through a $\pi \rightarrow \pi^*(NO_2)$ transition [5,6]. Excitations to the lower energy $2^1A''$ and $1^1A''$ states contribute to the longer wavelength absorption, the latter producing a shoulder on the strong absorption band peaking near 270 nm ($\sigma = 1.64 \times 10^{-20}$ cm^2) [4]. Both states result from exciting one electron from non-bonding O atom orbitals to the $\pi^*(NO_2)$ orbital [5,6].

Energetically, upon 248 nm excitation, HNO_3 could undergo three-bond cleavage reactions: OH + NO_2, O + HONO, or H + NO_3. [7] Previous work found the H + NO_3 channel to be negligible ($\Phi_{248}(H) = 0.002$) [8]. While dissociation to OH + NO_2 is clearly the dominant product channel, the branching to the O + HONO channel is in debate. The only direct O quantum yield measurement found $\Phi_{248}(O) = 0.031 \pm 0.010$ [8]. Turnipseed et al. used pulsed laser-induced fluorescence, calibrated to H_2O_2, to obtain absolute OH quantum yields for HNO_3 of $\Phi_{248}(OH) = 0.95 \pm 0.09$ and $\Phi_{193}(OH) = 0.33 \pm 0.06$ [8]. Work utilizing electron bombardment ionization at 193 nm found $\Phi_{193}(OH) = 0.33 \pm 0.04$ via photofragment translational spectroscopy, in agreement with the Turnipseed study [1]. In contrast, Schiffman et al. [3] measured OH quantum yields from HNO_3 with infrared flash kinetic spectroscopy, finding $\Phi_{248}(OH) = 0.75 \pm 0.10$ and $\Phi_{193}(OH) = 0.47 \pm 0.06$; this low 248 nm OH quantum

* Corresponding author. Fax: +1 773 702 5863.
E-mail address: ljb4@midway.uchicago.edu (L.J. Butler).

0009-2614/$ - see front matter © 2004 Elsevier B.V. All rights reserved.
doi:10.1016/j.cplett.2004.08.070

yield suggests another significant product channel. Until now, a photofragment translational spectroscopy measurement at 248 nm was precluded by the lower absorption cross section at this wavelength ($\sigma_{248} = 2.0 \times 10^{-20}$ cm^2) [4,9]. This study takes advantage of the low background associated with VUV photoionization, coupled with photofragment translational spectroscopy, to make an independent determination of the OH quantum yield at 248 nm.

2. Experimental

These photofragment translational spectroscopy experiments used a crossed laser-molecular beam scattering apparatus at Endstation 9.0.2.1 of the Advanced Light Source at the Lawrence Berkeley National Laboratory, described previously [10,11]. A pulsed molecular beam of 4% HNO_3 was generated by seeding 100% fuming HNO_3 (Spectrum Laboratory Products) at 5.5 °C in helium to a total backing pressure of 475 Torr. The mixture was expanded through a 0.5 mm diameter pulsed nozzle at 83 °C and photolyzed by a 248.5 nm KrF excimer laser. The photolysis beam was 225 mJ pulse^{-1}, focused onto a 10.4-mm^2 beam spot. The low HNO_3 absorption cross-section required a high laser fluence to see primary photoproducts, unavoidably causing secondary photodissociation of NO_2. The molecular beam typically peaked between 1488 and 1546 m/s, with a FWHM between 17% and 18.8%, as measured with a chopper wheel.

The velocity of the neutral photofragments is obtained from the time to travel 15.1 cm to the detector. There, they are ionized by tunable [12] vacuum-ultraviolet (VUV) synchrotron light and filtered by mass with a 2.1-MHz quadrupole (with a mass-dependent resolution from 0.3 to 0.45 amu) and a Daly detector. The time-of-flight constant, used to correct for the ion transit time, was 5.7 μs/amu$^{1/2}$. Higher harmonics of the synchrotron light were attenuated by an argon gas filter and, at wavelengths below 10.8 eV, a MgF_2 filter. At masses where this was insufficient, shot-to-shot subtraction of a laser-off, beam-on background was used.

3. Results

The data indicate that dissociation of HNO_3 into OH and NO_2 is the dominant primary dissociation channel following 248.5 nm excitation of HNO_3; we estimate that the O + HONO channel has no more than a 3% quantum yield. We looked for dissociation products which might give parent or daughter ion signal at $m/e = 16(O^+)$, $17(OH^+)$, $30(NO^+)$, $46(NO_2^+)$, $47(HNO_2^+)$, and $m/e = 63(HNO_3^+$; parent, to detect clusters).

The available energy (E_{avl}) following a photodissociation event is distributed amongst translational (E_T), rovibrational ($E_{v,r}$), and electronic (E_{el}) energy,

$$E_{avl} = E_{parent} + h\nu - D_0(HO\text{–}NO_2) = E_T + E_{v,r} + E_{el}, \quad (1)$$

where $D_0(HO\text{–}NO_2)$ is the bond dissociation energy, $h\nu$ is the photon energy (114.9 kcal/mol), and E_{parent} is taken as $\langle E_{vib}\rangle = 0.79$ kcal/mol at the nozzle temperature, as calculated from literature vibrational frequencies [13]. After secondary photodissociation of the NO_2,

$$E_{avl} = E_{parent} + 2h\nu - D_0(HO\text{–}NO_2) - D_0(O\text{–}NO) = E_{v,r} + E_{el} + E_T(OH + NO_2) + E_T(O + NO). \quad (2)$$

Formula 1 and a $D_0(HO\text{–}NO_2)$ of 47.5 ± 0.5 kcal/mol [7], give $E_{avl} = 68.2$ kcal/mol following the primary dissociation. After secondary photodissociation, $E_{avl} =$ 111.2 kcal/mol from formula 2 and a $D_0(O\text{–}NO)$ of 71.84560 ± 0.00015 kcal/mol [14].

We assigned signal at $m/e = 17(OH^+)$ (Fig. 1) to OH produced from $HO\text{–}NO_2$ bond fission in HNO_3, and derived the recoil kinetic energy distribution, $P(E_T)$, from forward convolution fitting of the data. The $P(E_T)$ is centered at 12 kcal/mol (Fig. 2). There was little or no evidence of products at $m/e = 46(NO_2^+)$, with an integrated signal of 44.5 ± 33 counts after 300 000 laser shots and 9 ± 19 counts after 150 000 laser shots at photoionization energies of 10.7 and 10.2 eV, respectively. This suggests that NO_2 may undergo secondary photodissociation and/or daughter ion fragmentation within the ionizer. Indeed, the $m/e = 16(O^+)$ data shows evidence of both these processes.

We could satisfactorily fit the $m/e = 16(O^+)$ data without assuming that $HNO_3 + h\nu \rightarrow O + HONO$ occurred (Fig. 3a). The slower peak is momentum-matched to the lower recoil kinetic energy portion of

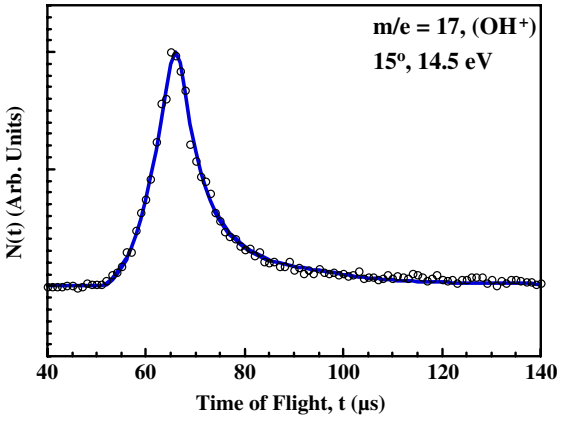

Fig. 1. TOF spectrum at $m/e = 17(OH^+)$, signal averaged for 600 000 laser shots at a 15° source angle and a 14.5-eV photoionization energy. We obtained the forward convolution fit to these data, shown with the solid line, from the $P(E_T)$ in Fig. 2. Open circles show experimental data.

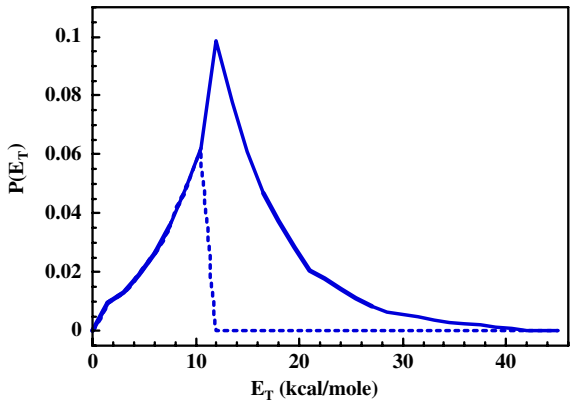

Fig. 2. The $P(E_T)$ for OH–NO_2 bond fission, derived from the forward convolution fit of the $m/e = 17(OH^+)$ spectra (Fig. 1), is given by the solid line. The small-dashed line shows the truncated $P(E_T)$ used in the forward convolution fit of $m/e = 16(O^+)$ signal as dissociative ionization of high E_{int} NO_2 photofragments (Fig. 3).

the data at $m/e = 17$, consistent with dissociative ionization of NO_2, and is fit with the $P(E_T)$ in Fig. 2, truncated at 12 kcal/mol. This cut-off, implying that only the higher internal energy NO_2 photofragments dissociatively ionize to O^+, corresponds to ~2.3 eV of NO_2 internal energy (see Section 4). Combined with the 15-eV photoionization energy, this provides 17.3 eV of energy to reach the O^+ ion, consistent with the appearance energy of O^+ from NO_2, reported as 16.8–17.6 eV [15].

The $P(E_T)$ generated to fit the faster peak in the $m/e = 16$ data, assigned to secondary photodissociation of NO_2 product, peaks at 17 kcal/mol but extends to 74 kcal/mol (Fig. 4). This signal is momentum-matched to the $m/e = 30$ data (Fig. 5), as NO and O are sibling co-fragments of NO_2 photodissociation. Thus, the same secondary $P(E_T)$ fits the data in both spectra. Although the fit shown for the $m/e = 30$ data includes no contribution from NO_2 dissociatively ionizing to NO^+ in the mass spectrometer, signal from 90 to 115 μs may be attributed to this source. Including this contribution does not substantially affect the $P(E_T)$ for the secondary dissociation channel. Although the primary dissociation channels were studied with an unpolarized laser, so the derived $P(E_T)$ does not depend on any anisotropy in the dissociation, in the fitting of the secondary channels we assumed the angular distribution was isotropoic.

We searched for evidence of the O + HONO product channel. No $m/e = 47(HONO^+)$ signal appeared above the background with photoionization at 11.5, 13.3, 14.3, and 16.3 eV. In the two spectra taken at 15.3 eV, integration of the $m/e = 47$ data over the time range of the slow NO peak (see below) resulted in a tiny integrated signal of 69 ± 38 counts after 250 000 laser shots and 94 ± 32 counts after 125 000 laser shots. The HONO photoionization energy was recently measured as 10.97 ± 0.03 eV [16], in agreement with computational results [17]. HONO gave strong daughter ions at

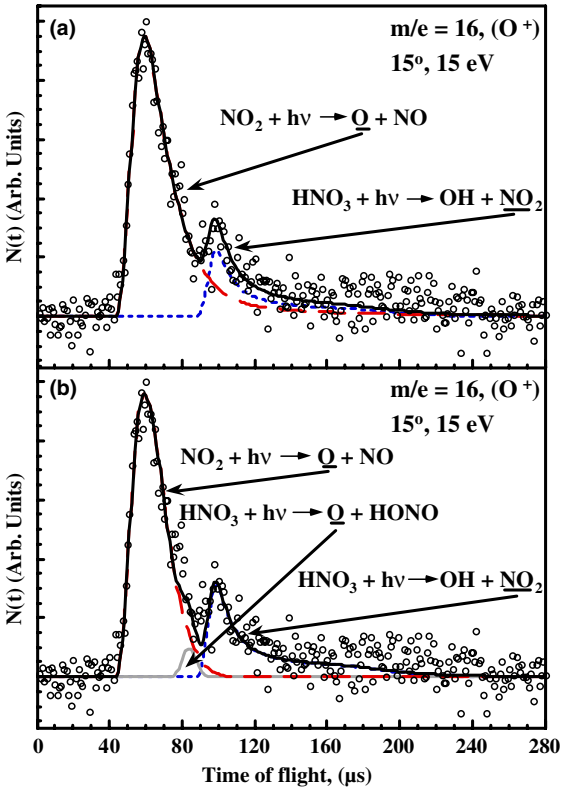

Fig. 3. TOF spectrum at $m/e = 16(O^+)$ at a 15° source angle and a 15-eV photoionization energy, signal averaged for 789 000 laser shots. Open circles show experimental data. (a) The forward convolution fit shown in the small-dashed line, calculated from the associated $P(E_T)$ in Fig. 2, corresponds to dissociative ionization of high E_{int} NO_2 photofragments. The forward convolution fit shown in the long-dashed line corresponds to secondary photodissociation of NO_2 to form NO + O; it was obtained from the $P(E_T)$ in Fig. 4. (b) Similar to (a) but adding an O + HONO channel, shown by the gray line, from a $P(E_T)$ peaked at 3.0 kcal/mol, with a FWHM of 1.7 kcal/mol. We deleted 3% of the low kinetic energy side of the $NO_2 \rightarrow NO + O P(E_T)$ in Fig. 4 to attribute the maximum possible O^+ signal to O + HONO. The appearance energy of NO^+ from HONO is unknown, so this fit assumes that all the HONO produced can give NO^+ daughter fragments.

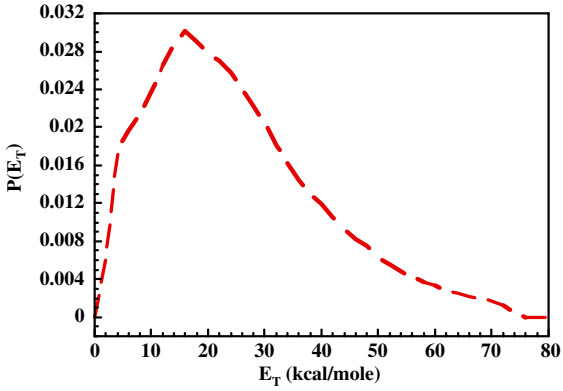

Fig. 4. The $P(E_T)$ for secondary photodissociation of NO_2, derived from the forward convolution fit of the $m/e = 16(OH^+)$ spectra (Fig. 3), is given by the long-dashed line.

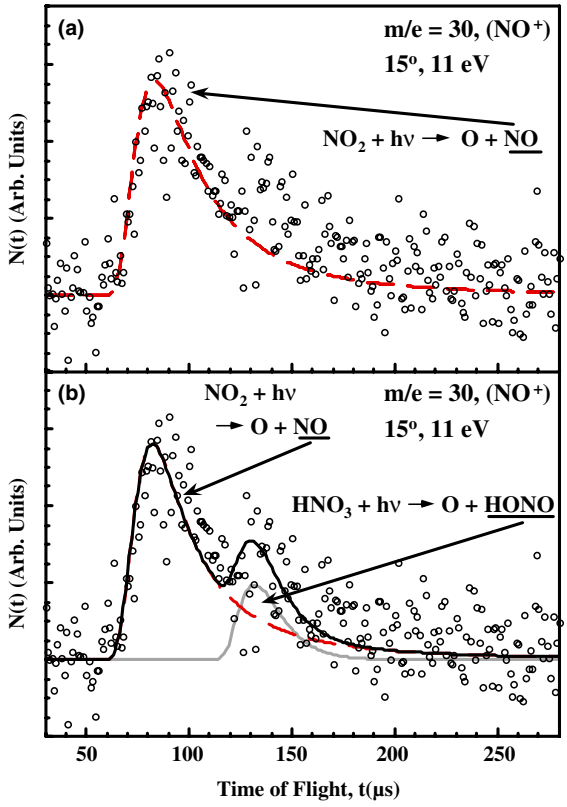

Fig. 5. TOF spectrum at $m/e = 30(NO^+)$ at a 15° source angle and a 11-eV photoionization energy, averaged for 700 000 laser shots. Potential contribution from dissociative ionization of NO_2 to NO^+ is not shown (see Section 3). (a) The forward convolution fit shown with the long-dashed line corresponds to the secondary photodissociation $P(E_T)$ from Fig. 4. Open circles indicate experimental data points. (b) Fit obtained when a 3% branching to O + HONO is allowed, as discussed for Fig. 3b. The gray line shows dissociative ionization of HONO to NO^+.

OH^+, O^+, NO^+, and NO_2^+ in a study of 193 nm HNO_3 photolysis with electron bombardment detection; [1] this 248 nm study showed little evidence of HONO at parent or any daughter ions following VUV photoionization. The $m/e = 30$ data showed a small apparent peak near 130 μs that was not fit by the $P(E_T)$ generated by the $m/e = 16$ data. The peak is too fast to obviously attribute to dissociating dimers; the absence of signal at the parent mass also suggests that no clusters were present. The NO^+ signal was too slow to assign to daughter ion fragmentation from $m/e = 46(NO_2^+)$, so we considered that the slow peak might be dissociative ionization of HONO. To ascertain the maximum possible branching to O + HONO, we used the $P(E_T)$ derived from the small peak at $m/e = 30$, assuming it was from the NO^+ daughter of HONO, to determine the expected arrival times of the momentum-matched O co-fragments in a modified $m/e = 16(O^+)$ fit (Fig. 3b). From this fit, which is not as good as that with no O + HONO contribution, an upper limit of 3% on the contribution from O + HONO was calculated. We conclude that the quantum yield of OH from 248 nm photolysis of HNO_3 is 0.97–1.0, assuming unit quantum yield for photodissociation.

4. Discussion

Photofragment translational spectra indicate that photodissociation of HNO_3 at 248 nm occurs primarily through the $OH + NO_2$ channel. As mentioned, this study was spurred by conflicting previous measurements of the quantum yield of OH at 248 nm; our results are in closer agreement with Turnipseed et al. [8] than Schiffman et al. [3]. In a previous HNO_3 photodissociation study at 193 nm, this laboratory also arrived at a result consistent with that of Turnipseed et al. [1]. The difference in $\Phi_{248}(OH)$ values for HNO_3 in the two spectroscopic studies arises from their disagreement over $\Phi(OH)$ for H_2O_2 at 248 nm. Schiffman et al. [3] measured the quantum yield from H_2O_2 as $\Phi_{248}(OH) = 1.58 \pm 0.23$ and $\Phi_{193}(OH) = 1.22 \pm 0.13$ while Turnipseed et al. used $\Phi_{248}(OH) = 2.00 \pm 0.05$ [18] and $\Phi_{193}(OH) = 1.51 \pm 0.18$ [19]. Despite extensive investigation of H_2O_2, no current $\Phi(OH)$ measurements resolve this discrepancy, as reviewed elsewhere [3,8]. If one adjusts the branching to $OH + NO_2$ at 248 nm reported by Shiffman et al. by using $\Phi_{248}(OH) = 2.0$ for 248 nm H_2O_2 photodissociation, their corrected quantum yield is 0.95, in agreement (within stated error bars) with our results here and those of Turnipseed et al. A similar correction cannot explain the disagreement at 193 nm.

This study also characterized the translational and internal energy distribution of the $OH + NO_2$ products. The $P(E_T)$ describing this channel peaks well away from zero at 12 kcal/mol. Myers et al. [1] constructed a restricted adiabatic correlation diagram linking HNO_3 electronic states to likely NO_2 products. This treatment [1,2] assumes a propensity towards electronic rearrangements that occur primarily within the NO_2 moiety and suggests that the $1^1A''$ state, which is likely to be accessed at 248 nm, correlates to $OH + NO_2$ (1^2A_2). However, it is also energetically possible to produce $NO_2(1^2B_1)$ via excitation to the $2^1A''$ state. From calculated vertical excitations, neither state [1] should generate a $P(E_T)$ peaked at 12 kcal/mol. Additionally, threshold energies for these states [20] indicate that they are energetically inaccessible at the high translational energy edge of the $P(E_T)$; thus, some ground state NO_2 is produced. We lack the sensitivity to assign NO_2 electronic states based on structure in the $P(E_T)$, as was possible at 193 nm.

We can compare the result here to a $P(E_{int})$ for the fluorescing portion of the NO_2 photoproduct from HNO_3 photolysis at 248 nm, measured by Miller and Johnson [9]. Although broader in shape than our distribution, that $P(E_{int})$ is also unimodal, peaking at ~54 kcal/mol NO_2 internal energy. For this to be consistent with the

current study, the OH fragment must have little internal excitation. Photodissociation of HNO_3 at wavelengths of 193 [21], 280 [22], 266 [23], and 241 nm [24] produced OH excitation, of only 3.3, 3.7, 3.7 and 3.0 kcal/mol, respectively. If 3 kcal/mol goes into OH, the distribution reported here would peak at E_{int} (NO_2) = 53 kcal/mol, similar to the Miller and Johnson study.

If the small peak at $m/e = 30$ corresponds to O + HONO, the only energetically accessible product channel is the spin-forbidden $HONO(X^1A') + O(^3P)$ [25,26]. Turnipseed et al. observed $O(^3P)$ atoms following 248 nm HNO_3 photolysis. Additionally, one channel in the 193 nm photolysis of HNO_3 was assigned to the spin-forbidden $O(^3P) + HONO(X^1A')$ by Li et al. [27] At higher energies, the spin-conserving product combination would be $O(^1D) + HONO(X^1A')$.

The crucial atmospheric role of HNO_3 motivates many studies [28]. This work shows that excitation to the $1^1A''$ state in the small shoulder near 270 nm results in a near unit OH + NO_2 quantum yield. The solar actinic flux in the stratosphere between 230 and 275 nm is low, resulting in only the red side of this absorption shoulder impacting stratospheric photochemistry on par with the 200 nm absorption to the $2^1A'$ state, as quantified by modeled HNO_3 photolysis rates [4,29].

Acknowledgements

The National Science Foundation supported this work under Grant No. CHE-0109588 (L.J.B.). M.J.K, M.C.R, and L.R.M. acknowledge a National Science Foundation Graduate Research Fellowship, Summer Environmental Research Award, and GAANN fellowship, respectively, for salary support. The Advanced Light Source is supported by the Director, Office of Science, Office of Basic Energy Sciences, Materials Sciences Division, of the US Department of Energy under Contract No. DE-AC03-76SF00098 at Lawrence Berkeley National Laboratory. The Chemical Dynamics Beamline is supported by the Director, Office of Science, Office of Basic Energy Sciences, Chemical Sciences Division of the US Department of Energy under the same contract.

References

[1] T.L. Myers, N.R. Forde, B. Hu, D.C. Kitchen, L.J. Butler, J. Chem. Phys. 107 (1997) 5361.
[2] N.R. Forde, T.L. Myers, L.J. Butler, Faraday Discuss. 108 (1997) 221.
[3] A. Schiffman, D.D. Nelson Jr., D.J. Nesbitt, J. Chem. Phys. 98 (1993) 6935, and references therein.
[4] F. Biaume, J. Photochem. 2 (1973) 139.
[5] Y.Y. Bai, G.A. Segal, J. Chem. Phys. 92 (1990) 7479.
[6] A.M. Graña, T.J. Lee, M. Head-Gordon, J. Phys. Chem. 99 (1995) 3493.
[7] J. Chase, W. Malcolm (Eds.), NIST-JANAF Thermochemical Tables, American Chemical Society, Washington, DC, 1998.
[8] A.A. Turnipseed, G.L. Vaghjiani, J.E. Thompson, A.R. Ravishankara, J. Chem. Phys 96 (1992) 5887.
[9] C.E. Miller, H.S. Johnston, J. Phys. Chem. 97 (1993) 9924.
[10] P.A. Heimann, M. Koike, C.W. Hsu, D. Blank, X.M. Yang, A.G. Suits, Y.T. Lee, M. Evans, C.Y. Ng, C. Flaim, H.A. Padmore, Rev. Sci. Instrum. 68 (1997) 1945.
[11] X. Yang, J. Lin, Y.T. Lee, D.A. Blank, A.G. Suits, A.M. Wodtke, Rev. Sci. Instrum. 68 (1997) 3317.
[12] The wavelength of the synchrotron light was tuned through changes in the gap of a U10 undulator, as calibrated in unpublished work by D. Peterka and M. Ahmed (2002).
[13] O.V. Dorofeeva, V.S. Irorish, V.P. Novikov, D.B. Neumann, J. Phys. Chem. Ref. Data 32 (2003) 879.
[14] R. Jost, J. Nygøard, A. Pasinski, A. Delon, J. Chem. Phys. 105 (1996) 1287.
[15] J.W. Au, C.E. Brion, Chem. Phys. 218 (1997) 109, and references therein.
[16] C.A. Taatjes, D.L. Osborn, T.A. Cool, K. Nakajima, Chem. Phys. Lett. 394 (2004) 19.
[17] D. Sengupta, R. Sumathi, S.D. Peyerimhoff, Chem. Phys. 248 (1999) 147.
[18] G.L. Vaghhiani, A.R. Ravishankara, J. Chem. Phys. 92 (1990) 996, The error bars of the value in this reference are different from those reported by the same group in [8].
[19] G.L. Vaghjiani, A.A. Turnipseed, R.F. Warren, A.R. Ravishankara, J. Chem. Phys. 96 (1992) 5878.
[20] G.D. Gillispie, A.U. Khan, A.C. Wahl, R.P. Hosteny, M. Krauss, J. Chem. Phys. 63 (1975) 3425.
[21] G.-H. Leu, C.-W. Hwang, I.-C. Chen, Chem. Phys. Lett. 257 (1996) 481.
[22] J. August, M. Brouard, J.P. Simons, J. Chem. Soc., Faraday Trans. 284 (1988) 587.
[23] S.J. Baek, C.R. Park, H.L. Kim, J. Photochem. Photobiol. A 104 (1997) 13.
[24] A. Sinha, R.L. Vander Wal, F.F. Crim, J. Chem. Phys. 91 (1989) 2929.
[25] C. Larrieu, A. Dargelos, M. Chaillet, Chem. Phys. Lett. 91 (1982) 465.
[26] C.E. Moore, Selected Tables of Atomic Spectra, National Standard Reference Data System, Washington, DC, 1976.
[27] Q. Li, R.T. Carter, J.R. Huber, Chem. Phys. Lett. 334 (2001) 39.
[28] J.H. Seinfeld, S.N. Pandis, Atmospheric Chemistry and Physics, Wiley, New York, 1998.
[29] O. Rattigan, E. Lutman, R.L. Jones, R.A. Cox, K. Clemitshaw, J. Williams, J. Photochem. Photobiol. A 66 (1992) 313.